Protonation of a Hydroxyl Anion Bridging Two Divalent Magnesium Ions in Water Probed by First Principles Metadynamics Simulations

ARTICLE *in* THE JOURNAL OF PHYSICAL CHEMISTRY B · SEPTEMBER 2010

Impact Factor: 3.3 · DOI: 10.1021/jp102991f

Protonation of a Hydroxide Anion Bridging Two Divalent Magnesium Cations in Water Probed by First-Principles Metadynamics Simulation

Jung Mee Park*,† and Mauro Boero‡

Department of Chemistry, Sungkyunkwan University, Suwon, Gyeonggi, 440-746, Korea, Institut de Physique et Chimie des Matériaux de Strasbourg, UMR 7504 CNRS and University of Strasbourg, 23, rue du Loess, F-67034 Strasbourg, France, and CREST, Japan Science and Technology Agency, Sanban-cho, Tokyo 102-0075, Japan

Received: April 2, 2010; Revised Manuscript Received: July 5, 2010

The protonation of a hydroxide anion (OH^-) located between two magnesium cations (Mg^{2+}) in aqueous solution has been investigated by first-principles metadynamics simulation. We observe that the complex $Mg^{2+}-OH^--Mg^{2+}$ is stabilized by the coparticipation of the hydroxide anion to the first hydration shells of both the Mg^{2+} cations. Contrary to the cases of OH^- in pure water, the transfer of protons in the presence of the divalent metal ions turns out to be a slow chemical event. This can be ascribed to the decreased proton affinity of the bridging OH^-. Metadynamics simulation, used to overcome the difficulty of the long time scale required by the protonation of the bridging OH^-, has shown that the system possesses a great stability on the reactant state, characterized by a bioctahedral (6,6) solvation structure around the two Mg^{2+} cations. The exploration of the free energy landscape shows that this stable bioctahedral configuration converts into a lower coordinated (5,6) structure, leading to a proton transfer from a water molecule belonging to the first solvation shell of the Mg^{2+} ion having the lower coordination to the bridging OH^-; the free energy barrier for the protonation reaction is 11 kcal/mol, meaning that the bridging hydroxide is a weak base. During the proton transfer, the bridging OH^- reverts to an H_2O molecule, and this breaks the electrostatic coupling of the two Mg^{2+} ions, which depart independently with their own hydration shells, one of which is entirely formed by water molecules. The second one carries the newly created OH^-. Our results show that the flexibility in the metal coordination plays a crucial role in both the protonation process of the bridging OH^- and the separation of the metal cations, providing useful insight into the nature of proton transfer in binuclear divalent metal ions, with several biological implications, such as, for instance, transesterification of catalytic RNA.

1. Introduction

In nature, metal ions are utilized to activate many enzymes that catalyze a large variety of biochemical reactions.[1−5] Understanding the solvation properties of metal ions, in particular when two (or more) cooperate, is of great importance for identifying their catalytic role in a large variety of aqueous and enzymatic chemical reactions. For instance, proton transfer through a solvent ligand, such as a water molecule or an OH^- anion, of a metal ion is one of the crucial activation processes performed by metal ions in many enzymatic hydrolysis reactions. A typical example is RNA hydrolysis, in which the deprotonation of a metal-bound water promotes phosphodiester-bond breaking by aiding the departure of the leaving group.[4,8,9] In many metalloenzymes containing a binuclear metal center, early dissociation of a water molecule shared by the first hydration shells of both metal cations and bridging them triggers the initial step of complex hydrolysis reactions.[2,3]

A metal-bound water molecule is known to have a lower pK_a with respect to bulk water.[5−7] This is generally explained by the electrostatic stabilization of the metal ion upon deprotonation of the metal-coordinated water, resulting in a departing proton and a metal-coordinated OH^-.[12] In this respect, a metal-bound OH^- is commonly assumed as an important ingredient to explain the reaction mechanism of metal-ion-catalyzed hydrolysis reactions. For instance, a hydroxide anion is supposed to trigger the nucleophilic attack in the RNA self-cleavage by the abstraction of a proton from the 2′-OH group at the active site of an RNA enzyme (ribozyme).[9] In some cases, to explain abnormally short distances in the metal−metal separations observed by X-ray crystallography in ribozymes, obtained under high pH conditions, a hydroxide anion is assumed to exist between the two metal cations.[10,11] Indeed, hydroxide-bridged binuclear metal clusters have been proposed as a putative catalytic unit in the active sites of many binuclear metalloenzymes,[13−27] and an OH^- located in the middle of binuclear metal centers is frequently assumed to replace a simple water molecule both because of its attractive Coulomb interaction with the two metal cations close to each other and because it represents a more suitable candidate to trigger a nucleophilic attack.[2] We must acknowledge that, although plausible, the presence of an OH^- remains experimentally elusive. Since only O atoms are crystallographically detectable, whether an OH^- or a water molecule is present between two divalent metal ions is still an open issue. Therefore, detailed information about free energy and (de)protonation pathways of a metal-bridging water and a metal-bridging hydroxide ion is of great importance to understand the reaction mechanism of metalloenzymes containing binuclear metal centers at their active sites.

* To whom correspondence should be addressed. E-mail: jungmee@skku.edu. Current address: School of Computational Science, Korea Institute for Advanced Study, Hoegiro 87, Dongdaemun-gu, Seoul 130-722, Korea.
† Sungkyunkwan University (SKKU).
‡ CNRS and University of Strasbourg, Japan Science and Technology Agency.

10.1021/jp102991f
Published on Web 08/09/2010

On the computational side, calculation of free energies and reaction pathways of complex chemical and biochemical processes in aqueous solutions has been, and in many respects still is, a challenge. First-principles molecular dynamics (FPMD)[28,29] combined with the metadynamics approach[30,31] has been proven to be a powerful tool to study rare events in solutions.[9,32−36] In the present work, in an attempt at understanding the protonation process of a biologically relevant system, we focus on the protonation process of a hydroxide anion bridging two magnesium cations (Mg^{2+}) in aqueous solution

$$[Mg{-}O^*H{-}Mg]^{3+} + H_2O \rightarrow [Mg{-}H_2O^*{-}Mg]^{4+} + OH^- \rightarrow 2Mg^{2+} + H_2O^* + OH^- \quad (1)$$

Mg^{2+} is one of the most common and versatile divalent metal counterions in biological systems.[1−5] According to both experiments[37−39] and theoretical studies[12,40,41] on Mg^{2+} in aqueous solutions, the Mg−O internuclear separation ranges from 2.0 to 2.2 Å, and the first solvation shell is constituted by six water molecules in an octahedral arrangement. While in proteins, Mg^{2+} tends to bind directly to side-chain ligands (inner-sphere mode), and in nucleic acids, it prefers to bind indirectly via one, or more, mediating H_2O molecule(s) (outer-sphere mode).[5] The protonation reaction (eq 1) of an aqueous metal-bridging OH^- goes through the formation of a metal-bridging water, generating, in turn, a terminal OH^- anion. As the reaction proceeds, the bridged metal complex is dissociated into two metal ions departing with their independent hydration shells. In comparison with a single Mg^{2+} in solution, very little is known about the bridged metal−hydroxide complex and its protonation reaction; specifically, questions arise about the stable solvation structure of the reactant, the details of the proton abstraction (i.e., whether or not a bridging OH^- abstracts a proton from a bulk (solvent) water molecule or from a metal-coordinated H_2O molecule), the effect of hydration shell(s) fluctuations, the exact location of the newly created OH^- (i.e., in the bulk solvent or within the metal-coordination sphere), and the relative stability between bridging OH^-/H_2O.

To provide an answer to these issues, we examine the solution structure and coordination fluctuations of the metal-bridging hydroxide complex via FPMD simulations. Then, we calculate free energies and protonation pathway of the metal-bridging hydroxide by performing a reactive FPMD simulation in the framework of the metadynamics approach.

2. Computational Details

2.1. Car−Parrinello MD. All simulations were performed within the Car−Parrinello molecular dynamics (CPMD) approach using the CPMD code.[28,29] The density functional theory used here to describe atomic interactions includes gradient corrections to the exchange and correlation functional after Hamprecht, Cohen, Tozer, and Handy (HCTH).[42] The accuracy of this functional to describe aqueous solution properties has already been assessed.[43] Valence-core interactions are described by norm-conserving pseudopotentials of the Troullier−Martins[44] type within a Kleinmann−Bylender integration scheme.[45] For Mg, nonlinear core corrections[46] were included, and cutoff radii of 1.104 and 1.343 Å were adopted for the *s* and *p* angular momenta, respectively. A density cutoff radius of 0.762 Å was chosen for the core correction. Valence electrons were represented in a plane wave basis set with an energy cutoff of 70 Ry, the convergence having been assessed on small Mg(II) systems and liquid water.[9] To ensure an accurate updating of the wave functions, while preserving the adiabaticity, we used a fictitious electronic mass of 400 au.[47,48] The time step was set to 4.0 au (0.097 fs). Simulations were performed for a system consisting of a single OH^- ion, two Mg^{2+} ions, and 73 water molecules in a cubic box of 13.146 Å length which corresponds to a density of 1.0 g/cm^3 with periodic boundary conditions. A metal-bridged OH^- located between two Mg^{2+} was first optimized in the gas phase and then solvated with 73 water molecules. An initial configuration for CPMD was obtained from classical molecular dynamics simulation at 300 K, fixing only the optimized metal-bridged OH^- moiety. As far as the CPMD simulation is concerned, the system was equilibrated at 300 K for ∼5 ps with a velocity scaling thermostat, and then a production run was carried out for ∼7 ps in the microcanonical ensemble.

2.2. Metadynamics. To simulate the protonation process of the aqueous metal-bridging hydroxide anion, the focus of this work, we make use of the Lagrangian metadynamics method.[31] In this scheme, the reaction time scale is accelerated by applying a systematic biasing potential according to a set of a few predefined collective variables (CVs) suited to describe the reaction mechanism. The biasing potential is defined as a sum of small repulsive Gaussian-shaped potentials having a preassigned Gaussian height w, a Gaussian width Δs_α, and centered on the (instantaneous) CV value, $\mathbf{s}(t)$

$$V_{\text{bias}}(\mathbf{s},t) = w \sum_{t' \le t} \exp\left(-\sum_\alpha \frac{(s_\alpha - s_\alpha(t'))^2}{2\Delta s_\alpha^2}\right) \quad (2)$$

Successive additions of Gaussians compensate the initial deep local minimum, allow the system to escape from it, and enhance the probability of sampling over the transition region on the configuration space by discouraging a resampling of the phase space already explored. In the metadynamics extended Hamiltonian, additional dynamical variables, s_α, are introduced for each collective variable, $S_\alpha(\mathbf{R})$, with a fictitious mass M_α and a harmonic spring coupling keeping these new dynamical variables bound to the analytic functions $S_\alpha(\mathbf{R})$ representing the CVs

$$H = H_0 + \sum_\alpha \left[\frac{1}{2}M_\alpha\left(\frac{ds_\alpha}{dt}\right)^2 + \frac{1}{2}k_\alpha(s_\alpha - S_\alpha(\mathbf{R}))^2\right] + V_{\text{bias}}(\mathbf{s},t) \quad (3)$$

With a proper choice for the parameters k_α, M_α, the Gaussian deposition rate, and the Gaussian size,[49] $-V_{\text{bias}}(\mathbf{s}, t)$ can be used as an estimate of the free energy profile for sufficiently long simulation times. In the present work, three collective variables were used. The first one is the coordination number of chemically bonded H atoms to the oxygen atom O* of the hydroxide anion, n_{O^*H}, varying from 1 (bridged OH^-) to 2 (protonated form of OH^-)

$$n_{O^*H} = \sum_{i=O^*, j\in H} \frac{1 - \left(\frac{r_{ij}}{r_c}\right)^p}{1 - \left(\frac{r_{ij}}{r_c}\right)^q} \quad (4)$$

where $p = 6$, $q = 12$, and $r_c = 1.27$ Å.

The second CV is the coordination number of O atoms of either water or OH^- around the two Mg^{2+}, n_{MgO}

$$n_{MgO} = \frac{1}{2}\sum_{i\in Mg}^{2}\sum_{j\in O}\frac{1-\left(\frac{r_{ij}}{r_c}\right)^p}{1-\left(\frac{r_{ij}}{r_c}\right)^q} \quad (5)$$

where $p = 6$, $q = 12$, and $r_c = 2.85$ Å. The third CV is the $Mg^{2+}-Mg^{2+}$ distance, r_{Mg-Mg}.

The parameters k_α and M_α were chosen on the basis of the fluctuations of the function $S_\alpha(\mathbf{R})$ at the equilibrium. For the three CVs, spring coupling constants, $k_1 = 0.6$, $k_2 = 0.08$, and $k_3 = 0.09$, and fictitious mass parameters, $M_1 = 150$, $M_2 = 20$, and $M_3 = 20$, were used. Gaussians were added every 140 time steps with their widths of $\Delta s_1 = 0.05$, $\Delta s_2 = 0.3$, and $\Delta s_3 = 0.35$ au, respectively, and sampling their amplitudes w uniformly in the range 0.12−0.8 kcal/mol. The temperature of the system was kept at 300 K by a velocity rescaling of the atomic velocity.

3. Results and Discussion

3.1. Solvation Structure, Dynamical Behavior, and Basicity of a Bridging OH^-. To examine the solvation structure and the dynamical behavior of the bridged metal−hydroxide complex, we performed a standard CPMD simulation for about ∼7 ps as explained in the computational details section, in view of a pre-equilibration prior to the metadynamics inspection. In Figure 1 we report the time evolution of the Mg−Mg and Mg−O* distances (panel (a)) and the Mg−O*−H* angles (panel (b)). We observe that the bimetallic complex $Mg^{2+}-OH^--Mg^{2+}$ is stable throughout our simulation. This stability is primarily maintained by the bridging OH^- which belongs simultaneously to the first hydration shells of both metal cations. The bridging OH^- plays the role of a Coulomb screen since it alleviates the electrostatic repulsion between the two adjacent positively charged Mg^{2+} cations and leads to a short-distance stabilization of the two metal ions. As shown in Figure 1(a), the Mg−Mg distances fluctuate around 3.86 ± 0.10 Å. Figure 1(b) shows that the bimetal structure motif forms a triangular geometry with an average Mg−O*−Mg angle of 141° ± 6° and a Mg−O*−H* angle of 107° ± 8°. These average structural properties are slightly different from the results of previous classical MD study,[10] which predicted a linear Mg−O*−Mg structure with a flat angle and resulting in slightly longer average Mg−Mg distances for a $Mg^{2+}-OH^-Mg^{2+}$ bound to the RNA backbone in a ribozyme. We attribute this difference to the point charge model approximation adopted in the classical simulations.

To analyze the solvation structure of the bridged metal hydroxide solute, we calculated the Mg−oxygen (g_{MgO}) radial distribution function from the simulation (Figure 2(a)). The first peak of the Mg−O radial distribution is splitted into a peak at 2.10 Å and a peak at 2.16 Å for the Mg−O* and Mg−O_w (O_w = water oxygen atom) distances, respectively, indicating that the magnesium−hydroxide interactions are stronger than the metal−water interactions. According to previous experimental and computational results for a hydrated $Mg^{2+}(H_2O)_6$, X-ray diffraction experiments[38] reported 2.09 ± 0.04 Å for the average value of the Mg−O distances, and FPMD simulation studies[40,41] predicted 2.13 Å. Our predicted value of 2.16 Å for Mg−O_w distances is slightly longer than previous computed values. This is presumably due to the fact that compared to the $Mg^{2+}(H_2O)_6$, in the metal hydroxide, the Mg−water interactions become slightly weaker because of polarization effects induced by coordination of both metal cations to a negatively charged hydroxide anion. The oxygen coordination number $n_{MgO}(r)$, as computed by integrating the g_{MgO}, at the first minimum of $g_{MgO}(r)$, i.e., 3 Å, indicates that the first solvation shell of each Mg^{2+} contains five water molecules and the OH^-, yielding a coordination number of six and an octahedral arrangement similar to the stable structure of a hydrated Mg^{2+}. The first-shell water molecules around the two Mg^{2+} ions are found to be tightly coordinated to Mg^{2+} ions, and this is clearly seen by the fact that no exchange of water molecules between the first solvation shell and outer H_2O molecules could be observed and that no variations of the coordination number occur along the whole simulation. On the basis of our simulation, it can be

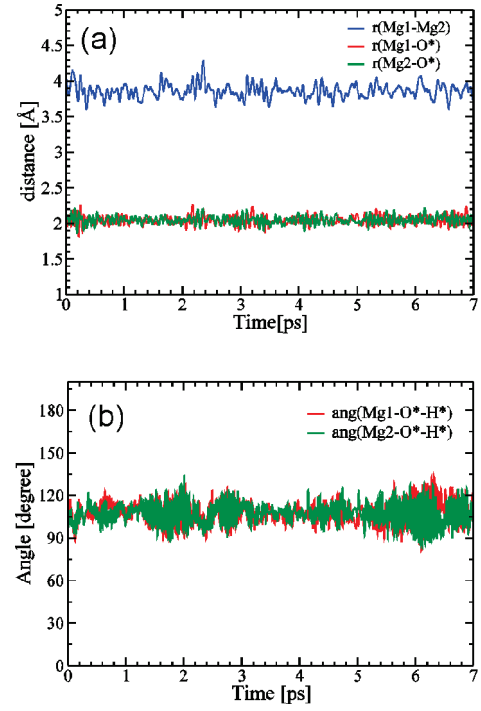

Figure 1. Time evolution of (a) the magnesium−magnesium (Mg−Mg) and magnesium−hydroxide oxygen (Mg−O*) distances and (b) the Mg−O*−H* angles of the bridged metal−hydroxide complex $Mg^{2+}-OH^-Mg^{2+}$.

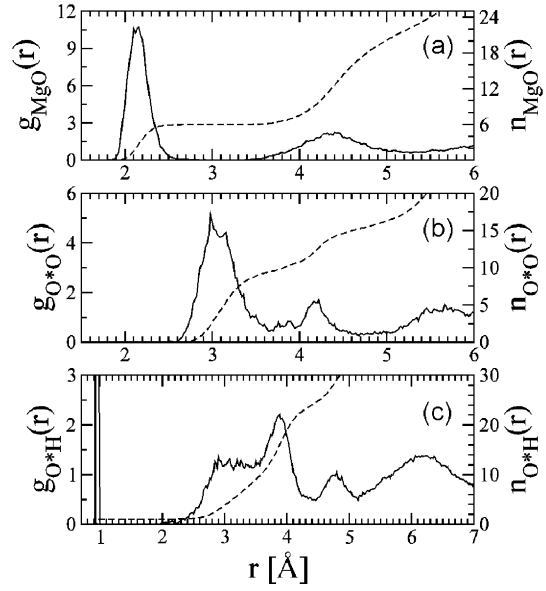

Figure 2. (a) Magnesium−oxygen (g_{MgO}), (b) hydroxide oxygen−oxygen (g_{O*O}), and (c) hydroxide oxygen−hydrogen (g_{O*H}) radial distribution functions (full lines) together with their corresponding coordination number integrals n (dashed lines).

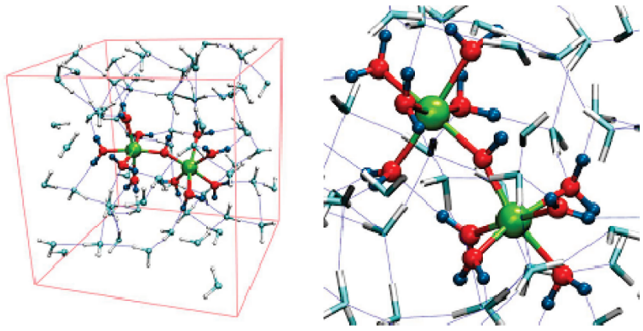

Figure 3. Stable solvation structure $[Mg(H_2O)_5{-}OH{-}Mg(H_2O)_5]^{3+}$ for the hydroxide anion bridging the two Mg^{2+} cations. (Left) The bioctahedral structure solvated in water. (Right) Close-up of the bioctahedral structure. Mg cations and O and H atoms of the stable bioctahedral structure are in green, red, and blue, respectively.

concluded that the stable solvation structure for a hydroxide anion bridging the two Mg^{2+} metal cations is a bioctahedral structure $[Mg(H_2O)_5{-}OH{-}Mg(H_2O)_5]^{3+}$ as displayed in Figure 3, which represents a stable local minimum on the free energy surface.

A feature worthy of note is the fact that the bridging OH^- does not give rise to any proton transfer on our picosecond time scale, contrary to what occurs in aqueous simulations of a free OH^- or terminal OH^-, in which the rates of proton transfer to the hydroxide anion are anomalously high, involving proton diffusion through hydrogen bond wires with negligible proton-transfer reaction barriers at room temperature.[50−52] The complete inactivity for proton transfer in our bimetal system can be explained by the greatly reduced basicity of the bridging OH^- as evidenced by the analysis for its local hydration structure with the hydroxide anion−oxygen (g_{O^*O}) and the hydroxide anion−hydrogen (g_{O^*H}) radial distribution functions plotted in Figure 2(b) and (c). In $g_{O^*O}(r)$, the first peak is located at about 3 Å which is much longer compared to the region of 2.4−2.6 Å in which the first peaks appear in bulk or terminal OH^- cases. By looking at $g_{O^*H}(r)$, it is evident that the hydrogen bonding interactions between OH^- and neighboring water molecules are missing since no peak exists at radial values corresponding to typical hydrogen bond distances. The distance between the hydroxide ion and the nearest neighboring hydrogen is about 2 Å, which is much longer than a hydrogen bond distance involving the hydroxide anion and corresponding to 1.6 Å. The coordination in the first hydration shell of our bridging OH^- is clearly reduced in comparison with the hypercoordination found for a free (or terminal) hydroxide anion, in which an OH^- can accept up to four water molecules as the most stable hydration structure.[50−52] The degree of reduction of the hypercoordination can be a quantitative measure of the degree of the reduced basicity with respect to an OH^- in the high dilution limit. Recent first-principles molecular dynamics simulations[52] for an excess OH^- in pure water reported that the running coordination number integrated from the O*−H radial distribution function (RDF) is 3.4, 3.9, and 4.0 if the integration is performed up to the first minimum for the RDF, depending on the PW91, BLYP, and HCTH functionals, respectively. In our Mg-bridging OH^-, this hypercoordination is greatly reduced to a value of 0.1, obtained also in our case from the O*−H running coordination number at the distance equal to the first minimum for a bulk OH^-. These results clearly point to the greatly reduced proton affinity of the bridging OH^- between the two metal ions. This very weak interaction with proton-donating water molecules leads to the inactivity observed for this bridging OH^- along the whole trajectory in our simulation.

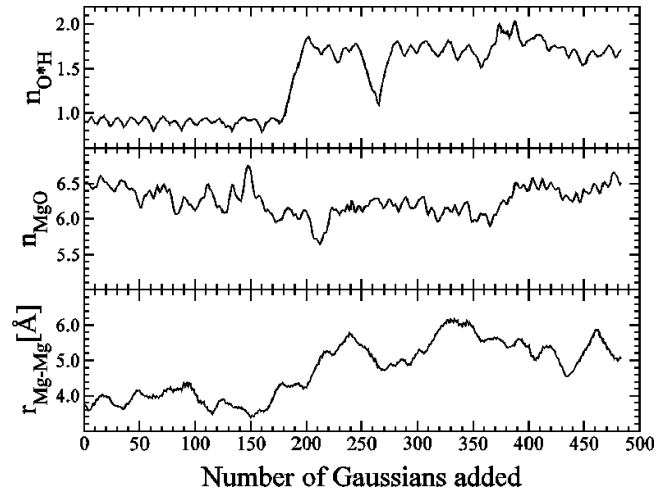

Figure 4. Collective variables $S_1(\mathbf{R}) = n_{O^*H}$, $S_2(\mathbf{R}) = n_{MgO}$, and $S_3(\mathbf{R}) = r_{Mg-Mg}$ obtained with the metadynamics simulation as a function of the number of Gaussian potentials that have been added to the system. The stride between subsequent Gaussians is 140 MD steps (= 13.6 fs).

3.2. Pathway and Free Energies of Protonation of a Bridging OH^-. The reduced proton affinity of the bridging OH^-, discussed above, suggests that to sample the pathway relevant to the protonation process of this OH^- a free energy sampling technique is required. Thus, we started our metadynamics simulation from the stable bioctahedral configuration obtained at the end of our Car−Parrinello run, using as Lagrangian additional variables the three collective variables described in the Computational Details section. The first collective variable, n_{O^*H}, is a natural choice for a proton transfer coordinate, based on chemical intuition. Instead of a proton transfer coordinate δ, the difference of two O−H distances between a shared proton as defined in ref 50, we choose n_{O^*H} because this analytic function defining the coordination number not only is sensitive to the O−H distance but also does not rely on any specific proton coming from a preassigned H^+ donor. Thus, the coordination number n_{O^*H} is more general in that it does not bias the protonation pathway in a specific direction. For the second collective variable, n_{MgO}, as mentioned in the previous section, the number of configurations accessible on the local minimum is limited to octahedral structures with six ligands for each Mg^{2+}. By taking the Mg−O coordination fluctuations into account with this collective variable, along with n_{O^*H}, we can explore other metal coordination configurations which are not accessible at the equilibrium but that may contribute to the activation of the protonation process. For the third collective variable, r_{Mg-Mg}, our preliminary short simulation has shown that a gradual increase of the Mg−Mg separation of the bridged complex allows the approach of neighboring solvent water molecules toward OH^-. This observation led to our third choice for the set of collective variables able to deal with any possible proton transfer. This allows us also to include the dissociation processes from the bridged form into two separated metal complexes, most likely resulting from the protonation of the bridging OH^-.

Figure 4 shows the evolution of the collective variables as a function of the number of Gaussians added during the metadynamics simulation. The collective variables fluctuate around $n_{O^*H} = 1.0$, $n_{MgO} = 6.0$, and $r_{Mg-Mg} = 3.8$ Å in the reactant state. After about 180 Gaussians, the reactant well is filled, and the system escapes into the product well in which the collective variables fluctuate around $n_{O^*H} = 2.0$, $n_{MgO} = 6.0{-}6.5$, and $r_{Mg-Mg} = 5.5$ Å.

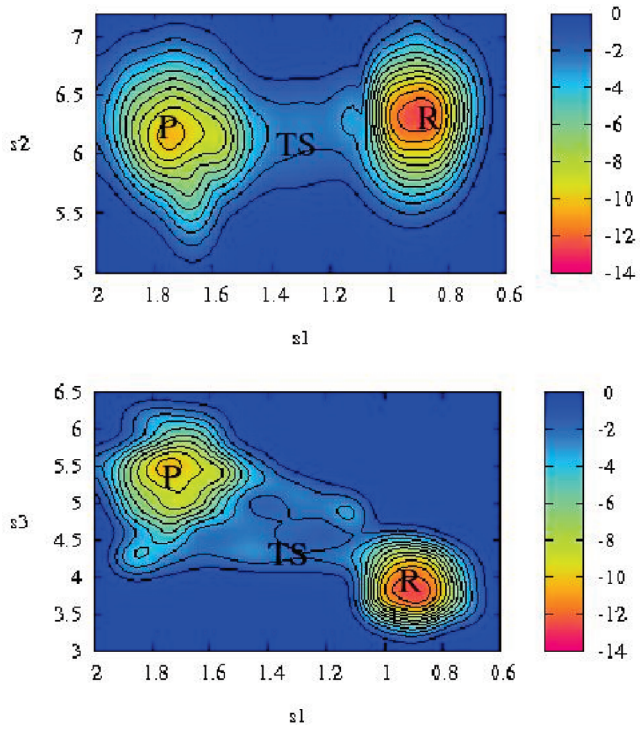

Figure 5. 2D projections $F(s_1,s_2)$ (upper pannel) and $F(s_1,s_3)$ (lower panel) of the computed 3D free energy surface $F(s_1,s_2,s_3)$ reconstructed from our metadynamics simulation for the protonation process of the bridging OH^-. The spacing between contour lines is equidistant and equal to 1 kcal/mol.

The resulting 3D free energy surface, $F(s_1, s_2, s_3)$ is represented in terms of two-dimensional contour density plots $F(s_1, s_2)$ and $F(s_1, s_3)$ by integrating over the remaining variables, s_3 and s_2, respectively, for better visualization in Figure 5. The free energy surface shows a deep and single-centered well (R) for the stable reactant state. From the minimum of the free energy surface corresponding to this reactant well up to the lowest maximum, along the free energy landscape, separating reactant (R) and product (P), a transition state (TS) region could be located for which we estimate a free energy barrier of 11 kcal/mol from a single free energy profile. To obtain a more accurate estimation of the barrier, one needs to compute an average of all the free energy profiles obtained for a full convergence in the phase space spanned by the selected collective variables[53] by continuing the simulation until these collective variables explore diffusively all the available regions of CV space, crossing backward and forward several times from the reactant to the product regions. In our case, as seen in Figure 4, the backward reaction is not observed since the reaction turns out to be irreversible. In solution, the two divalent metal cations are expected to diffuse away at the end of the process because of the strong Coulomb repulsion after the protonation. Hence, to be able to see multiple transitions between reactants and products for our system, a longer simulation by either limiting the maximum distance of the collective variable r_{Mg-Mg} or by reversing the momentum of the atom or group of atoms going too far away[54] is necessary. However, this would induce severe problems of momentum conservation, as explained in ref 54. As expected from the previous CPMD simulation, the energy barrier for the protonation of the bridging OH^- is much larger than that of a hydroxide anion in solution or of a terminal OH^-, for which protonation occurs spontaneously at room temperature, and is comparable with barriers characterizing weak bases.

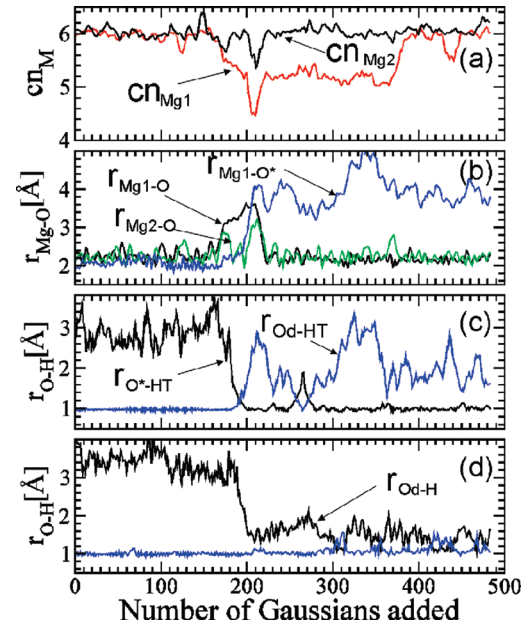

Figure 6. Time evolution of (a) the magnesium−oxygen coordination numbers cn_M (see definition in text), (b) the magnesium−oxygen coordination distances, and (c) the oxygen−hydrogen distances relevant to the protonation pathway for the bridging hydroxide ion as explored by the metadynamics simulation. O*, O_d, and H^T denote the bridging hydroxide anion oxygen, the proton−donor water oxygen, and the transferring proton, respectively, and (d) the oxygen−hydrogen distances characteristic of the proton-transfer attempts between the newly created terminal hydroxide anion oxygen (O_d) and its neighboring water oxygen.

The evolution of the metal coordination upon protonation can be seen from the trend of $F(s_1,s_2)$ in Figure 5 (upper panel). From the well-defined reactant minimum (R) in $F(s_1,s_2)$, one can notice that major configurations belonging to this well are characterized by a coordination number amounting to ~6 oxygens per Mg^{2+} cation. In contrast, configurations of the product well (P) are seemingly a mixture of various metal coordination numbers, still centered around 6, but with a larger dispersion, shifted toward lower coordination numbers. This distribution toward the lower Mg−O coordination region can be ascribed to the formation of new intermediates with lower metal coordinations, i.e., 5-fold or even 4-fold, during or after the proton transfer process.

These water rearrangements in the first solvation shell coupled with the proton transfer reaction can be better rationalized by an analysis of the metadynamics trajectory using a stiffer definition of the Mg−O coordination function cn_M (M = Mg_1 or Mg_2)

$$cn_M = \sum_{i=M, j\in O} \frac{1-\left(\frac{r_{ij}}{r_c}\right)^p}{1-\left(\frac{r_{ij}}{r_c}\right)^q},\ M = Mg_1 \text{ or } Mg_2 \qquad (6)$$

where $p = 10$, $q = 26$, and $r_c = 3.2$ Å. The result of this analysis is reported in panel (a) of Figure 6. From cn_M, as expected, the first solvation shell structure for the reactant state exhibits a stable bioctahedral structure with both Mg cations 6-fold coordinated ((6,6)-fold hereafter). After the addition of roughly 180 Gaussians, cn_{Mg1} decreases from 6 to 5, shortly before the transition state is reached (see also Figure 6(c)). Thus, it is

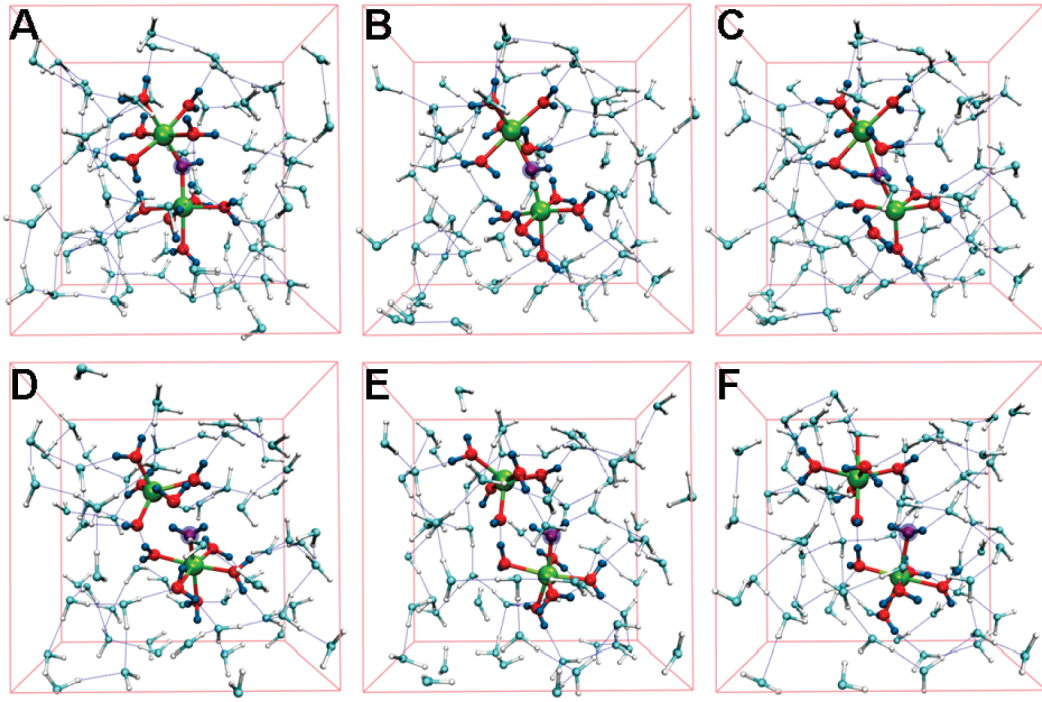

Figure 7. Representative snapshots for the protonation pathway of the bridging hydroxide anion as provided by our metadynamics trajectory shown for the stable reactant (A), the metal−water coordination breaking (B), the transition state (C), the high-energy distorted tetrahedral OH^- (D), the trigonal bipyramidal OH^- (E), and the octahedral OH^- product (F). The O atom of the bridging hydroxide anion is highlighted in blue. The other color codes are the same as in Figure 3.

evident that the loss of a water molecule belonging to the first hydration shell for one Mg^{2+} ion (Mg_1) initiates the proton transfer to the bridging OH^-. This implies that most of the free energy required for the protonation is spent on breaking a coordination bond between a Mg^{2+} cation and a water molecule in the first solvation shell rather than directly on breaking an OH bond of a proton-donating water molecule. Interestingly, our free energy barrier of 11 kcal/mol is comparable with the value of 7.4 kcal/mol[41] for the transformation from the 6-fold to the 5-fold coordination for an aqueous Mg^{2+} and the value of 9.5 kcal/mol for water exchange on $Mg(H_2O)_6^{2+}$ in ^{17}O NMR experiment.[55] If considering the inherent error from density functional theory and the error associated with the metadynamics run, our computed free energy barrier is in fair agreement with the available computational and experimental values. As mentioned above, the product state (P) of the reaction consists of various Mg−O coordinations. After the addition of about 200 Gaussians, shortly after the proton transfer reaction, a (4,5)-fold structure is temporarily realized by the two Mg^{2+} cations, Mg_1 and Mg_2, respectively. This structure transforms subsequently into a (5,6)-fold configuration. By continuing the addition of Gaussians, when they are about 380, the (5,6)-fold structure changes into a (6,6)-fold structure, thus recovering the octahedral configuration on both cations.

Figure 7 shows the most representative snapshots for the protonation pathway of the bridging OH^- as provided by our metadynamics trajectory. As discussed above, the reactant (A) in Figure 7A corresponds to the stable bimetal structure in the bioctahedral configuration. As Gaussians are added, the system starts to depart from the stable (6,6)-fold bioctahedral reactant state, visible in the increase of the Mg−O distances reported in Figure 6(b), which gives an idea of the coordination fluctuations. Occasionally, lower coordination solvation structures are formed such as (5,6)-fold or (5,5)-fold. Eventually, when a coordination between one of the two metal cations, specifically Mg_1, and a water molecule in the first solvation shell of Mg_1 is lost (Figure 7B), a water molecule in the first solvation shell of Mg_1 is able to form a hydrogen bond with the bridging OH^-, and subsequently, a proton can be transferred from the water molecule to the OH^-. This is represented by the transition state shown in Figure 7C. After the protonation, the bridging OH^- becomes a water molecule, whereas a newly created terminal OH^- is produced. The bimetal complex undergoes a dissociation, as shown by the increasing Mg−Mg distance r_{Mg-Mg} in the lowest panel of Figure 4 and in the snapshots of Figure 7D, E, and F.

During this protonation process, the system goes through a bridging-water state, between snapshots of Figure 7C and D, which is however rapidly lost. The instability of the bridging-water state is also reflected in the very shallow free energy surface at the region characterized by the collective variable ranges $1.8 < s_1 < 2.0$ and $4.0 < s_3 < 4.5$ in the free energy surface $F(s_1, s_3)$ (see Figure 5). Although the bridging-water state is just a transient configuration in our bimagnesium complex in pure water, in more complex systems, such as for instance RNA enzymes, the relative stability of the bridging water bound to a bimetallic complex with respect to the bridging hydroxide ion would be influenced by several factors such as the degree of water solvent exposure, the metal coordination(s) to residues of proteins and/or nucleic acids, and local partial charges of the metal ions in proximity of the biomacromolecules. Hence, in biological environment such as a highly folded enzyme pocket, the relative stability between bridging OH^- and bridging H_2O can be different, or even reversed, from that in aqueous solution, depending on the factors listed above. Since our computational scheme, applied here to the simple aqueous bi-Mg complex, can be easily applied to any biological system, it would be a useful tool to determine the relative stability between bridging OH^- and H_2O in bimetal-ion enzymes, a key issue for their activation.

As long as our metadynamics proceeds, the interaction between the bridging water molecule and Mg_1 becomes weaker, and the Mg_1−O* coordination breaks quickly (see Figure 6(b)),

generating a new intermediate shown in Figure 7D, where Mg_1 is 4-fold coordinated and a newly created OH^- appears; on the other hand, the second Mg^{2+} cation, Mg_2, is in a stable octahedral arrangement. This high-energy intermediate state D reverts into a more stable new intermediate E (Figure 7E) involving a 5-fold trigonal bipyramidal intermediate by taking an additional new Mg_1-O coordination. This 5-fold intermediate appears for about 2 ps during our metadynamics simulation, suggesting it is in a distinguishable local minimum in contrast with the case of the aqueous Mg^{2+} complex,[41] in which the 5-fold configuration was found to be a shallow local minimum separated from the global minimum of the 6-fold one by a barrier of about 2 kcal/mol. This enhanced stability of the 5-fold configuration of the Mg−hydroxide complex with respect to that of aqueous Mg^{2+} can be attributed to the effect that the OH^- coordination provides additional stabilization for the lower coordinated 5-fold configuration, as reported in the density functional study on hydrated magnesium−hydroxide clusters.[56] As the metadynamics simulation proceeds, this bipyramidal intermediate transforms into a square-pyramidal structure, and then Mg_1 coordinates another nearby solvent water molecule, forming a stable final product sketched in Figure 7F, resulting in an octahedral Mg^{2+} having a hydroxide ion in its first hydration shell and a second Mg^{2+} octahedral solvation structure including only water molecules. Contrary to the reduced proton affinity of the bridging OH^-, the terminal metal-bound OH^- recovers its proton affinity and strongly interacts with one or two neighboring hydrogen-bonded water molecule(s) as seen in Figure 7E and F accompanying the multiple proton-transfer attempts (see Figure 6(c) and (d)). A short standard MD simulation performed on one configuration belonging to this final product state indicates that this product state, in which the two Mg^{2+} cations are separated by two solvent molecules OH^- and H_2O, remains stable at least for about 1.5 ps with the hydrogen-bonding interaction between the metal-bound terminal OH^- and the other metal-bound water molecule. We note that due to the finite cell size our metadynamics simulation cannot proceed toward larger metal−metal separations which should be available at dilute solution. However, the range of metal−metal separations explored by our study is sufficiently extended to include all the distances relevant to reaction pathways typical for most biological systems containing a Mg^{2+} binuclear metal center.

4. Concluding Remarks

We have carried out first-principles molecular dynamics simulations of a hydroxide anion OH^- bridging two Mg^{2+} cations in aqueous solution in an attempt at providing insight into a bimetal−ion complex rather ubiquitous in nature and, in particular, in biological systems. Our calculations provide an atomic-level picture of the reaction path and the related energetic details for the protonation process of the bridging and tightly bound $-OH^-$ ligand. Car−Parrinello molecular dynamics results highlight that the $Mg^{2+}-OH^--Mg^{2+}$ complex is stable in a bioctahedral solvation structure in aqueous solution and that protonation process of the bridging OH^- is a slow chemical event due to the reduced basicity. Our metadynamics results demonstrate that the protonation of this bridging OH^- is triggered by the loss of one water molecule in the first solvation shell of one of the two Mg^{2+} cations.

With our solution model, we captured the essential picture in which the dynamical evolution of the coordination of the divalent metal ions of the complex is coupled to the protonation process. These results are likely to be relevant in a wide variety of biochemical systems.

Acknowledgment. We gratefully acknowledge insightful discussions with Atsushi Oshiyama and Masaru Tateno. Computer resources were provided by the Academic Computing and Communications Center, University of Tsukuba, and by the supercomputing center of KISTI. The work at SKKU was supported by grant no. KSC-2008-S03-0004 from Korea Institute of Science and Technology Information.

References and Notes

(1) Noodlemnan, L.; Lovell, T.; Han, W.-G.; Li, J.; Himo, F. *Chem. Rev.* **2004**, *104*, 459–508.
(2) Mitić, N.; Smith, S. J.; Neves, A.; Guddat, L. W.; Gahan, L. R.; Schenck, G. *Chem. Rev* **2006**, *106*, 3338–3363.
(3) Wilcox, D. E. *Chem. Rev.* **1996**, *96*, 2435–2458.
(4) Sigel, R. K. O.; Pyle, A. M. *Chem. Rev.* **2007**, *107*, 97–113.
(5) Cowan, J. A. *Biological Chemistry of Magnesium*; VCH: New York, 1995.
(6) Burgess, J. *Metal Ions in Solution*; Halsted Press: New York, 1978.
(7) Douglas, B.; McDaniel, D.; Alexander, J. *Concepts and Models of Inorganic Chemistry*; John Wiley & Sons: New York, 1994.
(8) Boero, M.; Terakura, K.; Tateno, M. *J. Am. Chem. Soc.* **2002**, *124*, 8949–8957.
(9) Boero, M; Tateno, M; Terakura, K; Oshiyama, A. *J. Chem. Theory Comput.* **2005**, *1*, 925–934.
(10) Hermann, T; Auffinger, P; Scott, W. G.; Westhof, E. *Nucleic Acids Res.* **1997**, *25*, 3421.
(11) Boero, M.; Park, J. M.; Hgiwara, Y.; Tateno, M. *J. Phys.: Condens. Matter* **2007**, *19*, 365217.
(12) Bernasconi, L.; Baerends, E. J.; Sprik, M. *J. Phys. Chem. B* **2006**, *110*, 11444–11453.
(13) Thoden, J. B.; Phillips, G. N. J.; Neal, T. M.; Raushel, F. M.; Holden, H. M. *Biochemistry* **2001**, *40*, 6989–6997.
(14) Maher, M. J.; Ghosh, M.; Grunden, A. M.; Menon, A. L.; Adams, M. W. W.; Freeman, H. C.; Guss, J. M. *Biochemistry* **2004**, *43*, 2771–2783.
(15) Cama, E.; Pethe, S.; Boucher, J.-L.; Han, S.; Emig, F. A.; Ash, D. E.; Viola, R. E.; Mansuy, D.; Christianson, D. W. *Biochemistry* **2004**, *43*, 8987–8999.
(16) Samples, C. R.; Howard, T.; Raushel, F. M.; DeRose, V. J. *Biochemistry* **2005**, *44*, 11005–11013.
(17) Chen, S.-L.; Fang, W.-H.; Himo, F. *J. Phys. Chem. B* **2007**, *111*, 1253–1255.
(18) Suarez, D.; Diaz, N.; Merz, K. M. J. *J. Am. Chem. Soc.* **2003**, *125*, 15324–15337.
(19) Cama, E.; Shin, H.; Christianson, D. W. *J. Am. Chem. Soc.* **2003**, *125*, 13052–13057.
(20) (a) Chen, S.-L.; Fang, W.-H.; Himo, F. *J. Phys. Chem. B* **2007**, *111*, 1253–1255. (b) Chen, S.-L.; Marino, T.; Fang, W.-H.; Russo, N.; Himo, F. *J. Phys. Chem. B* **2008**, *112*, 2494–2500.
(21) Yang, L.; Liao, R.-Z.; Yu, J.-G.; Liu, R.-Z. *J. Phys. Chem. B* **2009**, *113*, 6505–6510.
(22) Huai, Q.; Colicelli, J.; Ke, H. *Biochemistry* **2003**, *42*, 13220–13226.
(23) Schenk, G.; Gahan, L. R.; Carrington, L. E.; Mitić, N.; Valizadeh, M.; Hamilton, S. E.; de Jersey, J.; Guddat, L. W *Proc. Natl. Acad. Sci. U.S.A.* **2005**, *102*, 273–278.
(24) Zhan, C.-G.; Norberto de Souza, O.; Rittenhouse, R.; Ornstein, R. L. *J. Am. Chem. Soc.* **1999**, *121*, 7279.
(25) Zhan, C.-G.; Zheng, F. *J. Am. Chem. Soc.* **2001**, *123*, 2835–2838.
(26) Smoukov, S. K.; Quaroni, L.; Wang, X.; Doan, P. E.; Hoffman, B. M.; Que, L., Jr. *J. Am. Chem. Soc.* **2002**, *124*, 2595–2603.
(27) Hadler, K. S.; Tanifum, E. A.; Yip, S. H-. C.; Miti, N.; Guddat, L. W.; Jackson, C. J.; Gahan, L. R.; Nguyen, K.; Carr, P. D.; Ollis, D. L.; Hengge, A. C.; Larrabee, J. A.; Schenk, G. *J. Am. Chem. Soc.* **2008**, *130*, 14129–14138.
(28) Car, R.; Parrinello, M. *Phys. Rev. Lett.* **1985**, *55*, 2471–2474.
(29) *CPMD*, IBM Corp. 1990−2006: MPI für Festkörperforschung Stuttgart 1997−2001.
(30) Laio, A.; Parrinello, M. *Proc. Natl. Acad. Sci. U.S.A.* **2002**, *99*, 12562–12566.
(31) Iannuzzi, M.; Laio, A.; Parrinello, M. *Phys. Rev. Lett.* **2003**, *90*, 238302.
(32) Boero, M.; Ikeshoji, T.; Liew, C. C.; Terakura, K; Parrinello, M. *J. Am. Chem. Soc.* **2004**, *126*, 6280–6286.
(33) Park, J. M.; Laio, A.; Iannuzzi, M.; Parrinello, M. *J. Am. Chem. Soc.* **2006**, *128*, 11318–11319.
(34) Houk, K. N.; Gunaydin, H. *J. Am. Chem. Soc.* **2008**, *130*, 10036–10037.
(35) Blumberger, J.; Ensing, B.; Klein, M. L. *Angew. Chem., Int. Ed. Engl.* **2006**, *45*, 2893–2897.

(36) Rodríguez-Fortea, A.; Vilà-Nadal, L.; Poblet, M. J. *Inorg. Chem.* **2008**, *47*, 7745–7750.
(37) Caminiti, R.; Licheri, G.; Piccaluga, G.; Pinna, G. *Chem. Phys. Lett.* **1977**, *47*, 275.
(38) Marcus, Y. *Chem. Rev.* **1988**, *88*, 1475.
(39) Pye, C. C.; Rudolph, W. W. *J. Phys. Chem. A* **1998**, *102*, 9933.
(40) Lightstone, F. C; Schwegler, E.; Hood, R. Q.; Gygi, F.; Galli, G. *Chem. Phys. Lett.* **2001**, *343*, 549–555.
(41) Ikeda, T; Boero, M; Terakura, K. *J. Chem. Phys.* **2007**, *127*, 074503.
(42) Hamprecht, F. A.; Cohen, A. J.; Tozer, D. J.; Handy, N. C. *J. Chem. Phys.* **1998**, *109*, 6264.
(43) VandeVondele, J.; Mohamed, F.; Krack, M.; Hutter, J.; Sprik, M.; Parrinello, M. *J. Chem. Phys.* **2005**, *122*, 014515.
(44) Troullier, N.; Martins, J. L. *Phys. Rev. B* **1991**, *43*, 1993–2006.
(45) Kleinman, L.; Bylander, D. M. *Phys. Rev. Lett.* **1982**, *48*, 1425–1428.
(46) Louie, S. G.; Froyen, F.; Cohen, M. L. *Phys. Rev. B* **1982**, *26*, 1738–1742.
(47) Grossman, J. C.; Schewegler, E.; Draeger, E. W.; Gygi, F.; Galli, G. *J. Chem. Phys.* **2004**, *120*, 300.
(48) Kuo, I. -F. W.; Mundy, C. J.; McGrath, M. J.; Siepmann, J. I.; VandeVondele, J.; Sprik, M.; Hutter, J.; Chen, B.; Klein, M. L.; Mohamed, F.; Krack, M.; Parrinello, M *J. Phys. Chem. B* **2004**, *108*, 12990.
(49) Laio, A.; Rodríguez-Fortea, A.; Gervasio, F. L.; Ceccarelli Parrinello, M *J. Phys. Chem. B* **2005**, *109*, 6714–6721.
(50) Tuckerman, M. E.; Marx, D.; Parrinello, M. *Nature* **2002**, *417*, 925–929.
(51) (a) Chen, B.; Park, J. M.; Ivanov, I.; Tabacchi, G.; Klein, M. L.; Parrinello, M. *J. Am. Chem. Soc.* **2002**, *124*, 8534–8535. (b) Chen, B.; Ivanov, I.; Park, J. M.; Parrinello, M.; Klein, M. L. *J. Phys. Chem. B* **2002**, *106*, 12006–12016.
(52) Tuckerman, M. E.; Chandra, A.; Marx, D. *Acc. Chem. Res.* **2006**, *39*, 151–158.
(53) Laio, A.; Gervasio, F. L. *Rep. Prog. Phys.* **2008**, *71*, 126601.
(54) Boero, M.; Ikeda, T.; Ito, E.; Terakura, K. *J. Am. Chem. Soc.* **2006**, *128*, 16798–16807.
(55) Bleuzen, A.; Pittet, P. A.; Helm, L.; Merbach, A. E. *Magn. Reson. Chem.* **1997**, *35*, 765.
(56) Kluge, S.; Weston, J. *Biochemistry* **2005**, *44*, 4877–4885.

JP102991F